Cleaner and stronger: how 8-quinolinolate facilitates formation of Co(III)–thiolate from Co(II)–disulfide complexes

Marvelous, C.; Azevedo Santos, L. de; Siegler, M.A.; Fonseca Guerra, C.; Bouwman, E.

Dalton Transactions

ROYAL SOCIETY OF CHEMISTRY

PAPER

View Article Online
View Journal | View Issue

Cite this: *Dalton Trans.*, 2022, **51**, 11675

Cleaner and stronger: how 8-quinolinolate facilitates formation of Co(III)–thiolate from Co(II)–disulfide complexes†

Christian Marvelous, [a] Lucas de Azevedo Santos, [b] Maxime A. Siegler,[c] Célia Fonseca Guerra *[a,b] and Elisabeth Bouwman *[a]

Received 1st July 2022,
Accepted 12th July 2022

DOI: 10.1039/d2dt02106d

rsc.li/dalton

The formation of Co(III)–thiolate complexes from Co(II)–disulfide complexes using the anionic ligand 8-quinolinolate (quin$^-$) has been studied experimentally and quantum chemically. Two Co(II)–disulfide complexes $[Co_2(L^xSSL^x)(Cl)_4]$ (x = 1 or 2; L^1SSL^1 = 2,2′-disulfanediylbis(*N*,*N*-bis(pyridin-2-ylmethyl)ethan-1-amine; L^2SSL^2 = 2,2′-disulfanedylbis (*N*-((6-methylpyridin-2-yl)methyl)-*N*-(pyridin-2-ylmethyl) ethan-1-amine) have been successfully converted with high yield to their corresponding Co(III)–thiolate complexes upon addition of the ligand 8-quinolinolate. Using density functional theory (DFT) computations the d-orbital splitting energies of the cobalt–thiolate compounds $[Co(L^1S)(quin)]^+$ and $[Co(L^2S)(quin)]^+$ were estimated to be 3.10 eV and 3.07 eV, indicating a slightly smaller ligand-field strength of ligand L^2SSL^2 than of L^1SSL^1. Furthermore, the orientation of the quin$^-$ ligand in the thiolate compounds determines the stability of the thiolate complex. DFT computations show that the thiolate structure benefits from more electrostatic attraction when the oxygen atom of the quin$^-$ ligand is positioned *trans* to the sulfur atom of the $[Co(L^1S)]^{2+}$ fragment. Quin$^-$ is the first auxiliary ligand with which it appeared possible to induce the redox-conversion reaction in cobalt(II) compounds of the relatively weak-field ligand L^2SSL^2.

Introduction

Transition-metal ions and sulfur-based ligands may engage in electron-transfer processes, as both species are susceptible to redox changes.[1] Interaction of different disulfide ligands with copper(I) salts can be fine-tuned to obtain either the copper(I)–disulfide or corresponding copper(II)–thiolate complex.[2] This particular redox conversion of transition-metal disulfide and thiolate complexes has been studied for over two decades and in several instances appear to be reversible (Scheme 1).[3] In a typical reaction, one electron from each of two metal centres of a binuclear complex are transferred to the disulfide ligand. Consequently, the disulfide group is reduced into two thiolates, which then bind to the oxidized metal centres. The redox changes involved in the redox-conversion reaction is relatively rare as it requires no external oxidant or reductant.[4–6]

In recent years, the study of the redox-conversion reaction of disulfide and thiolate compounds has progressed from the copper-based system to other metal ions such as Mn, Fe, and Co.[7–11] The cobalt system in particular is interesting, as redox-conversion of cobalt-based systems is relatively underexplored. Currently, only a handful of reports describe the redox-conversion between cobalt(II)–disulfide and cobalt(III)–thiolate compounds induced chemically by addition or removal of halide ions, or by changing the solvent system.[8,10,12] Recently, we reported the redox-conversion of cobalt(II)–disulfide compounds to their corresponding cobalt(III)–thiolate compounds by the addition of the external ligand 2,2′-bipyridine (bpy).[13]

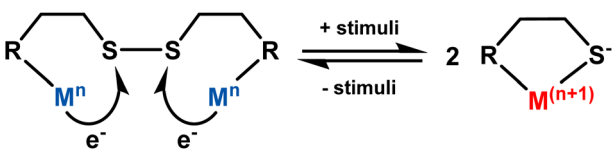

Scheme 1 Redox-conversion of metal-disulfide/metal-thiolate complex.

[a]*Leiden Institute of Chemistry, Gorlaeus Laboratories, Leiden University, P.O. Box 9502, 2300 RA Leiden, The Netherlands. E-mail: c.fonsecaguerra@vu.nl, bouwman@lic.leidenuniv.nl*

[b]*Department of Theoretical Chemistry, Amsterdam Institute of Molecular and Life Sciences (AIMMS), Amsterdam Center for Multiscale Modelling (ACMM), Vrije Universiteit Amsterdam, De Boelelaan 1083, 1081 HV Amsterdam, The Netherlands*

[c]*Department of Chemistry, Johns Hopkins University, 3400 N. Charles Street, Baltimore, Maryland 21218, USA*

†Electronic supplementary information (ESI) available: ESI-MS spectra, NMR spectra, table of crystallographic parameters for the crystal structures in the present work, detailed frontier orbital analyses, and Cartesian coordinates of optimized structures are provided. CCDC 2167787 ([$\mathbf{1_S}$]Cl), 2167788 ([$\mathbf{2_{SSquin}}$]) and 2167786 ([$\mathbf{2_S}$-Ag-$\mathbf{2_S}$]$(SbF_6)_3$). For ESI and crystallographic data in CIF or other electronic format see DOI: https://doi.org/10.1039/d2dt02106d

We hypothesized that the ligand-field strength of an added ligand would influence the formation of the cobalt(III)–thiolate complex, as cobalt(II)–disulfide complexes have a smaller d-orbital splitting energy than cobalt(III)–thiolate complexes. Addition of an external ligand can potentially increase the d-orbital splitting energy of the system, leading to a low-spin cobalt(II) species that readily transfers the single high-energy electron to the disulfide group, resulting in redox-conversion of cobalt(II)–disulfide to cobalt(III)–thiolate complexes. Unfortunately, bpy was found to be not suitable to induce this process.

In this manuscript we describe the results of our investigation on the effect of introducing 8-quinolinolate ($quin^-$) as the exogenous ligand to cobalt(II)–disulfide compounds of the ligands L^1SSL^1 (2,2′-disulfanediylbis(*N*,*N*-bis(pyridin-2-ylmethyl)ethan-1-amine) and L^2SSL^2 (2,2′-disulfanedylbis(*N*-((6-methylpyridin-2-yl)methyl)-*N*-(pyridin-2-ylmethyl)ethan-1-amine). The ligand L^1SSL^1 was chosen based on several examples of redox-conversion reactions using copper- and cobalt-based systems, which were successfully demonstrated to be triggered by various external factors such as halides, solvent, or temperature.[2,3,10–12,14] However, for the methylated ligand L^2SSL^2 the redox-conversion reaction has only been reported for the copper-based system in dichloromethane.[11] So far, we were unsuccessful in attempts to trigger redox conversion of cobalt(II)–L^2SSL^2 compounds,[12] warranting a more detailed investigation on how to overcome the low reactivity of these compounds. We hypothesized that the $quin^-$ ligand, which is expected to have a large ligand-field strength, may induce the redox-conversion reaction of Co(II)–disulfide of ligand L^1SSL^1 and L^2SSL^2 to their corresponding Co(III)–thiolate compounds. The anionic nature of $quin^-$ may also compensate for the dicationic charge of the resultant Co(III)–thiolate compounds and thus stabilize the relatively electron-poor Co(III) centre.

Results

Synthesis of the compounds

The ligands L^1SSL^1 and L^2SSL^2 were prepared according to published procedures[2,3,11] with slight modifications and were obtained in good yields. The synthesis and characterization of the disulfide compound $[Co_2(L^1SSL^1)(Cl)_4]$ ($[\mathbf{1_{SS}}]$) has been reported earlier.[10] The disulfide compound $[Co_2(L^2SSL^2)(Cl)_4]$ ($[\mathbf{2_{SS}}]$) was isolated as a purple powder in a yield of 72%. The ESI-MS spectrum of $[\mathbf{2_{SS}}]$ in methanol (Fig. S1†) shows peaks at *m*/*z* 777.1 and 376.2 corresponding to the species $[\mathbf{2_{SS}} - 2Cl^- + HCOO^-]^+$ and $[\mathbf{2_{SS}} - 4Cl^- + 2HCOO^-]^{2+}$, respectively (formic acid was used in the eluting solvent). The ^{1}H-NMR spectrum of $[\mathbf{2_{SS}}]$ dissolved in CD_3CN (Fig. S2†) shows large upfield and downfield shifts from −16 ppm up to 44 ppm, confirming the presence of paramagnetic Co(II) centres. Further characterization using a magnetic susceptibility balance revealed the value of the magnetic moment to be 3.98μ_B (calculated for each cobalt ion, spin-only magnetic moment 3.87μ_B), in agreement with the presence of two high-spin Co(II) centres within the binuclear molecule. Finally, elemental analysis shows that the compound $[\mathbf{2_{SS}}]$ was obtained analytically pure.

Addition of the ligand 8-quinolinol (Hquin) and triethylamine to solutions of *in situ* generated $[\mathbf{1_{SS}}]$ or $[\mathbf{2_{SS}}]$ afforded the mononuclear cobalt(III)–thiolate compounds $[Co(L^1S)(quin)]Cl$ ($[\mathbf{1_S}]Cl$) and $[Co(L^2S)(quin)]Cl$ ($[\mathbf{2_S}]Cl$) (Scheme 2). Both $[\mathbf{1_S}]Cl$ and $[\mathbf{2_S}]Cl$ were obtained in nearly quantitative yield (96% and 99%, respectively) as brown powders, and appeared to be hygroscopic. The ESI-MS spectrum of $[\mathbf{1_S}]Cl$ in methanol (Fig. S3†) shows a signal at *m*/*z* 461.1 corresponding to the cationic species $[\mathbf{1_S}]^+$. Similarly, the ESI-MS spectrum of $[\mathbf{2_S}]Cl$ in acetonitrile (Fig. S4†) shows a signal at *m*/*z* 475.3 corresponding to $[\mathbf{2_S}]^+$. The compounds $[\mathbf{1_S}]Cl$ and $[\mathbf{2_S}]Cl$ are diamagnetic both in the solid state as determined with a magnetic susceptibility balance as well as in solution as shown by the ^{1}H-NMR spectra (Fig. S5–S10†), in agreement with the presence of low-spin Co(III) ions. As the ^{1}H-NMR spectra showed that the compounds were pure but for the presence of triethylammonium chloride, we also carried out the synthesis in the absence of base. Indeed, both $[\mathbf{1_S}]Cl$ and $[\mathbf{2_S}]Cl$ can be synthesized in the absence of triethylamine; however the ^{1}H-NMR spectra (Fig. S11–S16†) then show the formation of unknown side products. Elemental analysis of both $[\mathbf{1_S}]Cl$ and $[\mathbf{2_S}]Cl$ shows that the compounds were obtained analytically pure after recrystallization. Single crystals of $[\mathbf{1_S}]Cl$ were grown using vapor diffusion of dry diethyl ether into a solution of $[\mathbf{1_S}]Cl$ in a 1 : 1 mixture of dry acetonitrile and dry methanol. Attempts to obtain single crystals of $[\mathbf{2_S}]Cl$ were not successful. Surprisingly, dark brown single crystals of a compound containing $[\mathbf{2_S}]^+$ were obtained after an anion-exchange reaction using vapor diffusion of dry diethyl ether into a dry acetonitrile solution containing $[\mathbf{2_S}]Cl$ and one equivalent of $AgSbF_6$. These single crystals turned out to be of the silver-bridged, dinuclear compound $[\{Co(L^2S)(quin)\}_2Ag(MeCN)](SbF_6)_3$ ($[\mathbf{2_S\text{-}Ag\text{-}2_S}](SbF_6)_3$).

Unexpectedly, in the NMR tube containing a CD_3CN solution of $[\mathbf{2_S}]Cl$ in high concentration, red single crystals were formed after some time, which turned out to be of the disulfide compound $[Co_2(L^2SSL^2)(quin)_2(Cl)_2]$ ($[\mathbf{2_{SSquin}}]$) as determined by X-Ray crystallography. Several crystallization attempts were performed to reproduce compound $[\mathbf{2_{SSquin}}]$, which indeed were successful. It was found that the crystals of $[\mathbf{2_{SSquin}}]$ are formed over time only in acetonitrile solution and

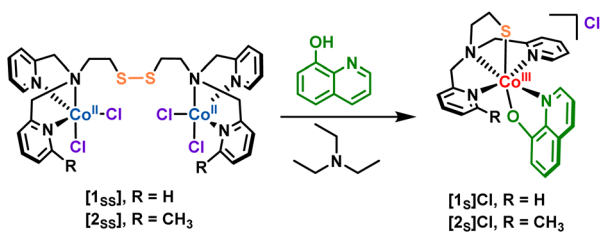

Scheme 2 Schematic representations of the cobalt compounds described in this work.

their formation appears to be concentration dependent. Crystals of [$\mathbf{2_{SSquin}}$] were not formed when the concentration of [$\mathbf{2_S}$]Cl in CH_3CN is smaller than 10 mg mL^{-1}, even over the period of one week. However, when the concentration of [$\mathbf{2_S}$]Cl is 50 mg mL^{-1}, crystals of [$\mathbf{2_{SSquin}}$] are formed within 5 hours. The infrared spectrum of the crystals of [$\mathbf{2_{SSquin}}$] (Fig. S17†) shows that indeed the compound is different from [$\mathbf{2_S}$]Cl. In addition, the solid-state diffuse reflectance spectrum of [$\mathbf{2_{SSquin}}$] (Fig. S18†) reveals absorption peaks at around 400 nm, 530 nm, and the onset of a third peak starting at 800–1000 nm, which are ascribed to charge transfer and d–d electronic transitions of Co(II) in an octahedral geometry.[15,16] Elemental analysis cannot be used to confirm the structure of the compound, as [$\mathbf{2_{SSquin}}$] is an exact dimer of [$\mathbf{2_S}$]Cl. It was found that [$\mathbf{2_{SSquin}}$] is readily soluble in methanol, but has limited solubility in acetonitrile or acetone. However, dissolution of compound [$\mathbf{2_{SSquin}}$] in these solvents regenerated [$\mathbf{2_S}$]Cl, as deduced from the ESI-MS and NMR spectra (Fig. S19–S21†).

Description of the crystal structures

Crystallographic data of the structures are provided in Table S1.† Compound [$\mathbf{1_S}$]Cl crystallizes in the triclinic space group $P\bar{1}$; the asymmetric unit contains one molecule of [$\mathbf{1_S}$]Cl and three lattice methanol solvent molecules. Selected bond distances and angles are provided in Table 1. The cobalt centre in [$\mathbf{1_S}$]Cl (Fig. 1a) is coordinated in an octahedral geometry by the sulfur donor and three nitrogen donor atoms of L^1S^-, as well as the oxygen and nitrogen donor atom of the $quin^-$ ligand. The octahedral geometry is slightly distorted, *i.e.* the largest deviation from perfect octahedral bond angles is 94.98(4)° for S1–Co1–N31. These small deviations are caused by the 5-membered chelate rings formed by the ligand L^1S^- and $quin^-$. The three nitrogen atoms of L^1S^- are arranged in a meridional fashion, similar to the structure of $[Co(L^1S)(NCS)_2]$.[10] The oxygen atom of the $quin^-$ ligand is located *trans* to the thiolate donor atom, whereas the nitrogen donor of the $quin^-$ ligand is *trans* to the tertiary amine of L^1S. The Co–S bond distance is 2.2324(4) Å, in agreement with other reports of low-spin cobalt(III)–thiolate compounds (2.19–2.30 Å, average bond distance = 2.252 Å).[8,10,17,18]

Table 1 Selected bond distances and bond angles in [$\mathbf{1_S}$]Cl

Atoms	distance (Å)	Atoms	Bond angles (°)
Co1–N1	1.9523(13)	S1–Co1–N1	90.22(4)
Co1–N11	1.9333(13)	S1–Co1–N11	93.91(4)
Co1–N21	1.9231(13)	S1–Co1–N21	89.47(4)
Co1–N31	1.9317(13)	S1–Co1–N31	94.98(4)
Co1–O1	1.9638(11)	S1–Co1–O1	176.70(4)
Co1–S1	2.2324(4)	O1–Co1–N1	89.53(5)
Co1–Cl1	6.3536(5)	O1–Co1–N11	89.33(5)
		O1–Co1–N21	87.24(5)
		O1–Co1–N31	85.29(6)
		N1–Co1–N11	84.00(5)
		N1–Co1–N21	85.98(5)
		N1–Co1–N31	174.78(5)
		N31–Co1–N11	95.24(5)
		N31–Co1–N21	94.44(5)
		N21–Co1–N11	169.43(6)

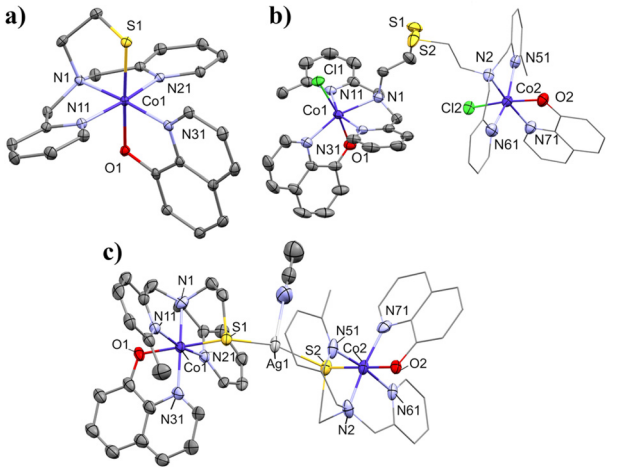

Fig. 1 Displacement ellipsoid plots (50% probability level) of (a) $[\mathbf{1_S}]^+$, (b) [$\mathbf{2_{SSquin}}$], and (c) $[\mathbf{2_S\text{-}Ag\text{-}2_S}]^{3+}$ at 110(2) K. Parts of the binuclear molecule are displayed as wireframe for clarity. Hydrogen atoms, counter ions, disordered molecules, and lattice solvent molecules are omitted for clarity. The methyl groups in [$\mathbf{2_{SSquin}}$] found at sites of minor occupancy have been removed for clarity.

The distance between the non-coordinated chloride ion and the cobalt ion is 6.3536(5) Å. The chloride ion is in close proximity of three lattice methanol solvent molecules, tightly held by hydrogen bond interactions. The closest intermolecular distance between two thiolate sulfur atoms is 6.648 Å. The distance between two cobalt centres in the unit cell is 9.851 Å.

Compound [$\mathbf{2_{SSquin}}$] crystallizes in the monoclinic space group $P2_1/n$. The structure of [$\mathbf{2_{SSquin}}$] (Fig. 1b) is partly disordered, as the methyl groups in L^2SSL^2 are located partially on each of the two pyridine rings. The occupancy factors of the major positions of the disorder refine to 0.782(6) and 0.744(6). In the asymmetric unit, one dinuclear molecule and one lattice solvent acetonitrile are co-crystallized. Each cobalt(II) centre is in a distorted octahedral geometry, bound to three nitrogen atoms of the ligand L^2S, the oxygen and nitrogen donor of one 8-quinolinolate ligand, and one chloride ion. The structure of this dinuclear compound resembles that of $[Co_2(L^1SSL^1)(bpy)_2(Cl)_2](BPh_4)_2$ reported in our previous study,[13] but in contrast to $[Co_2(L^1SSL^1)(bpy)_2(Cl)_2](BPh_4)_2$, the nitrogen donors of L^2SSL^2 are arranged in a meridional fashion, similar to the conformation in [$\mathbf{1_S}$]Cl. The chloride ion is coordinated *trans* to the oxygen donor of the $quin^-$ ligand, and the $quin^-$ nitrogen atom is *trans* to the tertiary amine of L^2SSL^2.

Selected bond distances and angles are listed in Table 2. The bond distances and bond angles related to the Co2 centre are very similar to those of Co1. The S–S bond distance in [$\mathbf{2_{SSquin}}$] is 2.0223(19) Å, comparable to that in $[Co_2(L^1SSL^1)(bpy)_2(Cl)_2](BPh_4)_2$ (2.029 Å). The Co–Cl bond distances (2.3921(7) Å for Co1–Cl1 and 2.4120(7) Å for Co2–Cl2) are longer than that in $[Co_2(L^1SSL^1)(bpy)_2(Cl)_2](BPh_4)_2$ (2.38 Å) or the disulfide

Table 2 Selected bond distances and angles in [2_{SSquin}]

Atoms	distance (Å)	Atoms	Bond angles (°)
Co1–N1	2.200(2)	O1–Co1–Cl1	171.43(6)
Co1–N11	2.192(2)	O1–Co1–N1	85.64(8)
Co1–N21	2.179(2)	O1–Co1–N11	87.30(8)
Co1–N31	2.132(2)	O1–Co1–N21	93.15(8)
Co1–O1	2.0610(19)	O1–Co1–N31	78.97(8)
Co1–Cl1	2.3921(7)	Cl1–Co1–N1	102.14(6)
S1–S2	2.0223(19)	Cl1–Co1–N11	90.70(6)
Co1–S1	5.848(1)	Cl1–Co1–N21	92.09(6)
		Cl1–Co1–N31	93.92(7)
		N1–Co1–N11	78.45(8)
		N1–Co1–N21	77.49(9)
		N1–Co1–N31	161.88(9)
		N31–Co1–N11	110.02(9)
		N31–Co1–N21	93.75(9)
		N21–Co1–N11	155.83(9)

compound [$\mathbf{1_{SS}}$] (2.324 Å and 2.272 Å), indicating that the Co–Cl bond is relatively weaker, possibly due to a *trans* effect of the quin$^-$ oxygen donor. The Co–N (tertiary amine nitrogen) bond distances are unusually long (2.200 Å and 2.199 Å) compared to those in other compounds with similar coordination spheres (octahedral Co(II) with four nitrogen donor atoms, one oxygen donor atom and one chloride ion), which are on average 1.952 Å.[19,20] The distances between the cobalt centres and the nearest disulfide sulfur atom are around 5.8 Å, which is slightly shorter than in [$\mathbf{1_{SS}}$] (5.961 and 5.937 Å). The structure does not contain hydrogen bonds, but a short intermolecular contact of 3.340 Å between the methylated pyridine ring and the neighbouring non-methylated pyridine ring indicates the presence of π–π stacking interactions. These π–π stacking interactions are in the parallel displaced conformation, most likely due to the different substituents (–CH_3 *vs.* –H) in the interacting moieties.[21]

A displacement ellipsoid plot (50% probability) for [$\mathbf{2_S}$-Ag-$\mathbf{2_S}$]$(SbF_6)_3$ is depicted in Fig. 1c (as the 3+ cation). Selected bond distances and bond angles are provided in Table 3. The bond distances and bond angles around the Co2 centre are similar to those of Co1. Compound [$\mathbf{2_S}$-Ag-$\mathbf{2_S}$]$(SbF_6)_3$ crystallizes in the monoclinic space group $P2_1/c$. In the asymmetric unit, one cationic molecule [$\mathbf{2_S}$-Ag-$\mathbf{2_S}$]$^{3+}$ is co-crystallized with three SbF_6^- counter ions and one lattice acetonitrile solvent molecule. The cationic fragment [$\mathbf{2_S}$-Ag-$\mathbf{2_S}$]$^{3+}$ is composed of two [$\mathbf{2_S}$]$^+$ complexes bridged by a silver ion to which one acetonitrile molecule is coordinated. The cobalt centres in the two [$\mathbf{2_S}$]$^+$ fragments are in slightly distorted octahedral geometries similar to [$\mathbf{1_S}$]$^+$, coordinated by one oxygen, one sulfur, and four nitrogen atoms. The Co–S bond distances are 2.2500(19) and 2.2612(19) Å, in agreement with a low-spin Co(III)–thiolate compound. The Ag^+ ion is in a T-shaped geometry; the S–Ag bond distances are 2.452(3) and 2.4300(28) Å, the S1–Ag–S2 bond angle is 157.5(2)°. The S–Ag bond distances in [$\mathbf{2_S}$-Ag-$\mathbf{2_S}$]$(SbF_6)_3$ are typical, as compared to other structures with similar geometries having an average S–Ag bond distance of 2.413 Å.[22–25]

Table 3 Selected bond distances and bond angles in [$\mathbf{2_S}$-Ag-$\mathbf{2_S}$]$(SbF_6)_3$

Atoms	distance (Å)	Atoms	Bond angles (°)
Co1–S1	2.2500(19)	S1–Co1–O1	176.4(4)
Co1–O1	1.919(7)	S1–Co1–N1	90.23(18)
Co1–N1	1.943(6)	S1–Co1–N11	88.73(17)
Co1–N11	2.020(5)	S1–Co1–N21	92.49(17)
Co1–N21	1.953(5)	S1–Co1–N31	95.4(4)
Co1–N31	1.934(7)	O1–Co1–N1	91.1(4)
S1–Ag1	2.452(3)	O1–Co1–N11	88.1(5)
S2–Ag1	2.4300(18)	O1–Co1–N21	91.0(5)
Ag1–N91	2.527(10)	O1–Co1–N31	83.7(5)
		N1–Co1–N11	84.5(2)
		N1–Co1–N21	83.4(2)
		N1–Co1–N31	170.6(4)
		N31–Co1–N11	103.1(3)
		N31–Co1–N21	88.8(3)
		N21–Co1–N11	167.9(2)
		S1–Ag1–S2	157.5(2)
		S1–Ag1–N91	112.7(2)
		S2–Ag1–N91	89.3(2)

Solution studies of Co(II)–disulfide and Co(III)–thiolate compounds

Addition of 8-quinolinol together with triethylamine into solutions of the disulfide compounds [$\mathbf{1_{SS}}$] or [$\mathbf{2_{SS}}$] results in an immediate colour change from purple to dark brown. The UV–visible spectrum of [$\mathbf{1_{SS}}$] in acetonitrile (Fig. 2a, solid blue line) is in accordance with the literature,[10] and matches the simulated spectrum (details are provided in the Experimental section) (Fig. 2a, dashed blue line). The spectrum of [$\mathbf{2_{SS}}$] (Fig. 2b, solid blue line) is red-shifted compared to that of [$\mathbf{1_{SS}}$]. The two peaks in the spectrum of [$\mathbf{2_{SS}}$] are located at 545 nm (1.5×10^3 M^{-1} cm^{-1}) and 652 nm (8.5×10^2 M^{-1} cm^{-1}), and are ascribed to Co(II) d–d transitions reflecting a trigonal–bipyramidal geometry.[15,16] Another Co(II) d–d transition is also visible at around 850–900 nm ($\varepsilon < 100$ M^{-1} cm^{-1}). The simulated spectrum of [$\mathbf{2_{SS}}$] (Fig. 2b, dashed blue line) has a reasonable match with the experimental spectrum, as the main features of the experimental spectrum are present.

The UV–visible spectra of dark brown solutions of [$\mathbf{1_S}$]Cl (Fig. 2a, black line) and [$\mathbf{2_S}$]Cl (Fig. 2b, black line) show peaks at 412 nm ($\varepsilon = 2.1 \times 10^4$ M^{-1} cm^{-1}) and 424 nm ($\varepsilon = 2.0 \times 10^4$ M^{-1} cm^{-1}), respectively, ascribed to a ligand-to-metal charge transfer transition (LMCT), most likely originating from the thiolate sulfur or quin$^-$ nitrogen donor.[18,26] The simulated spectra of [$\mathbf{1_S}$]Cl (Fig. 2a, dashed black line) and [$\mathbf{2_S}$]Cl (Fig. 2b, dashed black line) confirm that both absorptions indeed originate from LMCT transitions.

Computational studies

The role of the ligand-field strength of the additional ligand in the redox conversion of the Co(II)–disulfide complex with the LSSL ligand scaffold was previously reported.[13] In order to further validate the previous findings, we investigated the ligand-field strength of quin$^-$ using DFT to estimate the d-orbital splitting energies of the Co(III)–thiolate complexes. The structures of the cationic compounds [$\mathbf{1_S}$]$^+$ and [$\mathbf{2_S}$]$^+$ were optimized in low-spin singlet states ($S = 0$) in accordance with

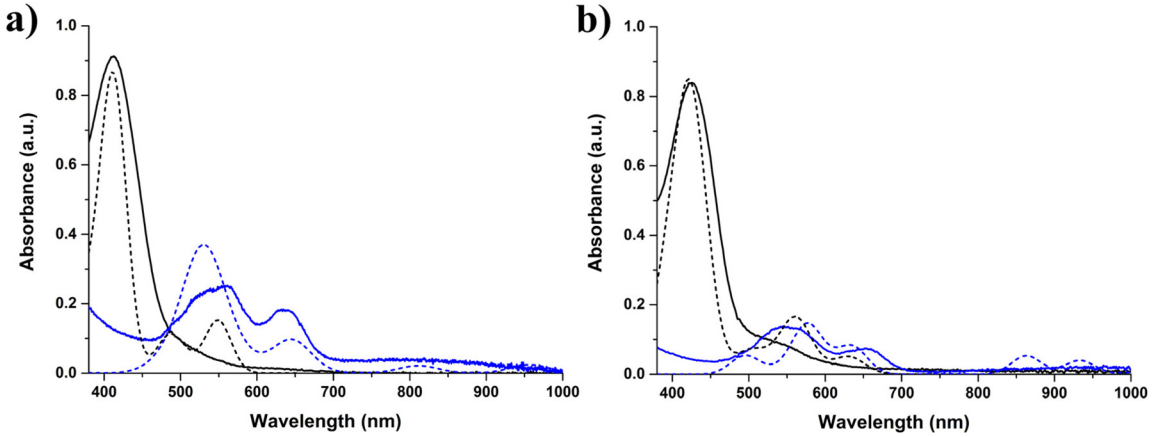

Fig. 2 UV-visible spectra of (a) 2 mM solution of $[\mathbf{1}_{SS}]$ (solid blue line) and 1 mM solution of $[\mathbf{1}_{S}]Cl$ (solid black line) in acetonitrile and (b) 2.5 mM solution of $[\mathbf{2}_{SS}]$ (solid blue line) and 1 mM solution of $[\mathbf{2}_{S}]Cl$ (solid black line) in acetonitrile. Simulated spectra of the respective compounds are provided as dashed lines; the wavelength of the simulated spectra has been adjusted for clarity. UV-visible spectra were recorded using a transmission dip probe with path length of 0.14 mm. Simulated spectra were generated using TDDFT calculations.

the experimental data. In addition, we were interested to investigate the influence of ligand ($quin^-$) orientation on the stability of the cobalt(III)–thiolate complex, as the conformation of the LS ligand scaffold has been shown to affect how the sulfur atom may approach the cobalt centre. Therefore, geometry optimizations were also done for both cationic compounds in which the orientation of $quin^-$ is reversed, so that the nitrogen donor atom is *trans* to the thiolate sulfur, and the oxygen atom *trans* to the tertiary amine nitrogen ($[\mathbf{1}_{S,rev}]^+$ and $[\mathbf{2}_{S,rev}]^+$). The equilibrium geometries in the gas phase for $[\mathbf{1}_{S}]^+$ and $[\mathbf{1}_{S,rev}]^+$ with selected bond distances are depicted in Fig. 3. Equilibrium geometries for $[\mathbf{2}_{S}]^+$ and $[\mathbf{2}_{S,rev}]^+$ in the gas phase are provided in Fig. S22.†

The cationic compounds $[\mathbf{1}_{S}]^+$ and $[\mathbf{2}_{S}]^+$ in methanol are about 5 to 6 kcal mol^{-1} more stable than $[\mathbf{1}_{S,rev}]^+$ and $[\mathbf{2}_{S,rev}]^+$, in agreement with the experimental results. The same trend in stability is observed in gas phase, *i.e.* without solvent $[\mathbf{1}_{S}]^+$ and $[\mathbf{2}_{S}]^+$ are about 7 to 9 kcal mol^{-1} more stable than $[\mathbf{1}_{S,rev}]^+$ and $[\mathbf{2}_{S,rev}]^+$. Thus, the preference in orientation of $quin^-$ is not determined by the media. The gas-phase equilibrium geometries of $[\mathbf{1}_{S}]^+$ and $[\mathbf{2}_{S}]^+$ are in good agreement with the geometries found in the crystal structures. The Co–S bond distances in the optimized structures of $[\mathbf{1}_{S}]^+$ or $[\mathbf{2}_{S}]^+$ are 2.225–2.226 Å, and the Co–O and Co–N bond distances are all within error range of those found in the crystal structures.

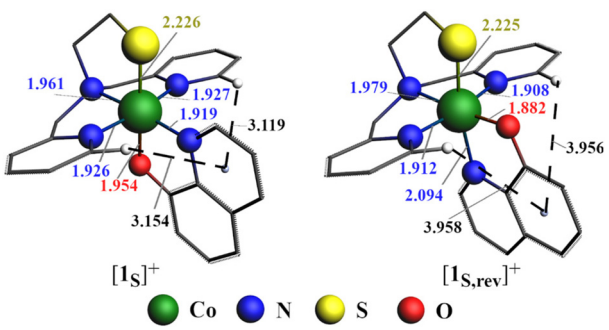

Fig. 3 Equilibrium geometries of $[\mathbf{1}_{S}]^+$ and $[\mathbf{1}_{S,rev}]^+$ in gas phase with selected bond distances (in Å). Hydrogen atoms are omitted for clarity, except for hydrogen atoms of $[Co(L1S)]^{2+}$ facing $quin^-$ ligand. The closest distances between the *ortho*-hydrogen atoms of the pyridine groups and the centre of the nearest $quin^-$ ring are depicted as dashed lines.

Attempts were undertaken to estimate d-orbital splitting energies of both $[\mathbf{1}_{S}]^+$ and $[\mathbf{2}_{S}]^+$ using the DFT method described in our previous report.[13] For both $[\mathbf{1}_{S}]^+$ and $[\mathbf{2}_{S}]^+$, five non-degenerate molecular orbitals were found with large Co d-orbital contributions (Fig. S23 and S24†). These five non-degenerate molecular orbitals are distributed in two sets of energy levels roughly corresponding to the expected t_{2g} and e_g levels for octahedral ligand-field splitting. The energy difference between the highest and the lowest of these MO levels of $[\mathbf{1}_{S}]^+$ is slightly larger (by 0.2 eV) than that of $[Co(L^1S)(bpy)]^{2+}{}_{mer}$, indicative of a larger ligand-field strength of $quin^-$ compared to bpy.[13] The energy difference of $[\mathbf{2}_{S}]^+$'s MO sets in a quantitative level is 3.07 eV, which is only slightly smaller than that of $[\mathbf{1}_{S}]^+$ (3.10 eV), indicating weaker ligand-field strength of the ligand L^2SSL^2 compared to that of L^1SSL^1. However, care should be taken with such quantitative comparisons, as the five orbitals in the MO sets comprises not only large contributions of the Co d-orbitals, but also of the donor atoms of the ligands.

In order to explain the stability of $[\mathbf{1}_{S}]^+$ compared to $[\mathbf{1}_{S,rev}]^+$, and analogously of $[\mathbf{2}_{S}]^+$ compared to $[\mathbf{2}_{S,rev}]^+$, we investigated the $[Co(L^1S)]^{2+}\cdots[quin]^-$ bond formation using activation strain analysis.[27,28] The bond energy (ΔE_{bond}) is given by eqn (1) and can be decomposed into the strain energy (ΔE_{strain}) and interaction energy (ΔE_{int}) (eqn (2)). The ΔE_{strain} is the energy needed to deform the fragments from their equilibrium geometries to their actual geometry in the complex. The ΔE_{int} term corresponds to the energy change when the deformed fragments are interacting with each other in the complex. We

observed that ΔE_{strain} of both $[\mathbf{1_S}]^+$ and $[\mathbf{1_{S,rev}}]^+$ are very similar (with 0.8 kcal mol^{-1} difference), and therefore does not cause the stabilization of $[\mathbf{1_S}]^+$ over $[\mathbf{1_{S,rev}}]^+$ (see Table 4). Instead, the interaction energy ΔE_{int} of $[\mathbf{1_S}]^+$ is more stabilizing by 8.2 kcal mol^{-1} than that of $[\mathbf{1_{S,rev}}]^+$. Thus, the interaction between the two fragments $[Co(L^1S)]^{2+}$ and $[quin]^-$ defines the stabilization of $[\mathbf{1_S}]^+$ over $[\mathbf{1_{S,rev}}]^+$.

$$\Delta E_{bond} = E_{complex} - E_{optimized[Co(L^1S)]^{2+}} - E_{optimized[quin]^-} \quad (1)$$

$$\Delta E_{bond} = \Delta E_{strain} + \Delta E_{int} \quad (2)$$

$$\Delta E_{int} = \Delta V_{elstat} + \Delta E_{Pauli} + \Delta E_{oi} \quad (3)$$

Next, we decomposed ΔE_{int} into Pauli repulsion energy (ΔE_{Pauli}), electrostatic interaction energy (ΔV_{elstat}), and orbital interaction energy (ΔE_{oi}), using energy decomposition analysis (eqn (3)).[28,29] The ΔV_{elstat} represents the Coulomb interaction between the unperturbed charge distributions of the two deformed fragments, which is usually an attractive interaction. ΔE_{Pauli} comprises of the destabilization energy associated with the interaction between occupied orbitals which is responsible for steric repulsion. The stabilizing ΔE_{oi} accounts for the charge-transfer, donor–acceptor interactions, and polarization. The molecular orbital diagram for the bonding interaction between $[Co(L^1S)]^{2+}$ and $[quin]^-$ is provided in Fig. S25–S26.† It is apparent from Table 4 that the electrostatic interaction ΔV_{elstat} plays the most important role in stabilizing $[\mathbf{1_S}]^+$ over $[\mathbf{1_{S,rev}}]^+$, as ΔV_{elstat} is about 21 kcal mol^{-1} lower for $[\mathbf{1_S}]^+$ than for $[\mathbf{1_{S,rev}}]^+$.

The molecular electrostatic potential of both $[Co(L^1S)]^{2+}$ and $[quin]^-$ fragments in $[\mathbf{1_S}]^+$ and $[\mathbf{1_{S,rev}}]^+$ are shown in Fig. 4. It was found that in both $[\mathbf{1_S}]^+$ and $[\mathbf{1_{S,rev}}]^+$ the positive charges are evenly spread out over the $[Co(L^1S)]^{2+}$ fragment. In $[quin]^-$ both the nitrogen and the oxygen atom are more negatively charged but the negative charge is delocalized over the carbon atoms of the aromatic rings. Therefore, the attraction between $[Co(L^1S)]^{2+}$ and $[quin]^-$ fragments is not only determined by the electrostatic interaction between the neighbouring atoms but has a significant contribution from long-range interactions between the $[Co(L^1S)]^{2+}$ and $[quin]^-$ fragments. This is demonstrated by the distances of the *ortho*-hydrogen atoms of the pyridine rings to the aromatic ring in the $quin^-$ ligand (Fig. 3) which are shorter in $[\mathbf{1_S}]^+$ (3.154 Å and 3.119 Å) than in $[\mathbf{1_{S,rev}}]^+$ (3.958 Å and 3.956 Å).

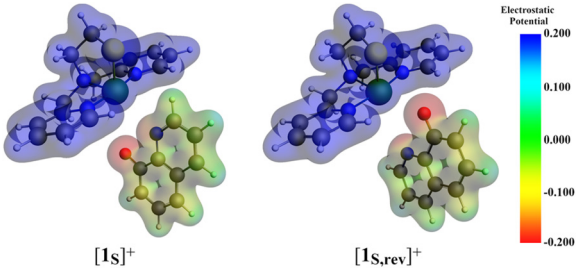

Fig. 4 Electrostatic potential of $[Co(L^1S)]^{2+}$ and $[quin]^-$ fragments in $[\mathbf{1_S}]^+$ and $[\mathbf{1_{S,rev}}]^+$.

Table 4 Energy terms derived from energy decomposition analysis of $[\mathbf{1_S}]^+$ and $[\mathbf{1_{S,rev}}]^+$

	Energy (kcal mol^{-1})	
	$[\mathbf{1_S}]^+$	$[\mathbf{1_{S,rev}}]^+$
$\Delta E_{bond,methanol}$	−61.7	−55.7
ΔE_{bond}	−238.5	−229.6
ΔE_{strain}	12.4	13.2
ΔE_{int}	−251.0	−242.8
ΔV_{elstat}	−290.2	−269.1
ΔE_{Pauli}	183.6	159.8
ΔE_{oi}	−144.4	−133.4

Discussion

We try to gain understanding of the influence of the ligand-field strength of the additional ligands on the redox-conversion of cobalt(II)–disulfide compounds based on our LSSL scaffold. In our previous report, we described our study using the external ligand 2,2′-bipyridine (bpy) in combination with the compound $[Co_2(L^1SSL^1)(X)_4]$ (X = Cl, Br).[13] Unexpectedly, the reaction with bpy turned out to be not straightforward, as the ligand-field strength of bpy appeared to be not as large as was anticipated.[13,30] In the current study we employed a similar strategy, but now using the bidentate ligand 8-quinolinolate. In addition to exerting a strong ligand-field this ligand is anionic in nature, which might help stabilizing the charge of the cobalt(III)–thiolate fragment.

Indeed, our experimental results show that the addition of $quin^-$ to both cobalt(II)–disulfide compounds $[\mathbf{1_{SS}}]$ and $[\mathbf{2_{SS}}]$ affords their respective cobalt(III)–thiolate compounds $[\mathbf{1_S}]Cl$ and $[\mathbf{2_S}]Cl$ in a clean manner, in contrast to the reactions with bpy in which several side products were observed. Remarkably, the crystal structure of $[\mathbf{2_{SSquin}}]$ shows that the L^2S fragment binds with the three nitrogen donor atoms in meridional arrangement, whereas in $[Co_2(L^1SSL^1)(bpy)_2(Cl_2)](BPh_4)_2$ the nitrogen donor atoms are in a facial arrangement.[13] We argued that formation of the cobalt(III)–thiolate compound with bpy is hampered by the fact that several donor atoms of the chelating ligands in this 'intermediate' compound have to dissociate and rearrange before redox conversion can take place. In addition, DFT calculations showed that the highest singly occupied molecular orbital (SOMO) of the facial isomer of the 'intermediate' bpy compound is more stabilized than that of the meridional isomer; thus making it more difficult for electron transfer to occur in the experimentally observed 'intermediate' with facial arrangement of the nitrogen donor atoms.[13]

In the present study, we observed a concentration-dependent equilibrium between $[\mathbf{2_{SSquin}}]$ and $[\mathbf{2_S}]Cl$ (Scheme 3). It appears that when the concentration of the cobalt(III)–thiolate species $[\mathbf{2_S}]Cl$ is sufficiently large, the shorter distances

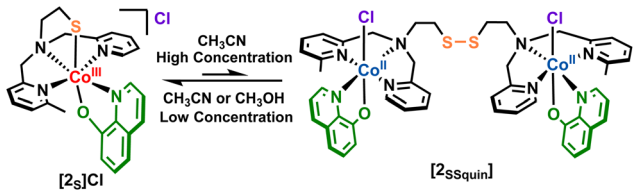

Scheme 3 Concentration-dependent equilibrium between $[\mathbf{2_S}]Cl$ and $[\mathbf{2_{SSquin}}]$.

between cobalt(III)–thiolate molecules allow for the formation of the dimer $[\mathbf{2_{SSquin}}]$. It is evident that this process only occurs at higher concentrations and is a relatively slow process, as the ^{1}H NMR spectra of $[\mathbf{2_S}]Cl$ are in agreement with a diamagnetic thiolate compound (Fig. S8–S10†). ESI-MS spectra of $[\mathbf{2_{SSquin}}]$ (Fig. S19†) can only be recorded for low concentration solutions and also show a signal corresponding to $[\mathbf{2_S}]^+$ (Fig. S4†). The ESI-MS spectrum (Fig. S19†) does not show the presence of a dimeric species, indicating that the reverse process, *i.e.* formation of $[\mathbf{2_S}]Cl$ from $[\mathbf{2_{SSquin}}]$, occurs more rapidly in low concentrations. The meridional arrangement of the L^2S ligand combined with the orientation of $quin^-$ in the structure of $[\mathbf{2_{SSquin}}]$ provides space after dissociation of the chloride ions for the disulfide sulfur atom to approach the cobalt(II) centre for electron transfer, to ultimately form the cobalt(III)–thiolate species $[\mathbf{2_S}]Cl$.

The introduction of two methyl groups in the ligand L^2SSL^2 has been shown to result in longer Co–N distances,[2,11,12] indicating a decrease of the donor ability of the methylated pyridine nitrogen atom, resulting in lower ligand-field strength, thus decreasing the chances of redox conversion of its cobalt(II)–disulfide compound to the corresponding cobalt(III)–thiolate complex.[12] The red-shifts of about 10 nm in the UV-visible spectra of $[\mathbf{2_{SS}}]$ or $[\mathbf{2_S}]Cl$ compared to $[\mathbf{1_{SS}}]$ or $[\mathbf{1_S}]Cl$, respectively, indicate that indeed the ligand L^2SSL^2 has a lower ligand-field strength than L^1SSL^1. This is confirmed by the results of our DFT studies: the energy difference of the highest and lowest MO in the set of orbitals with large cobalt d-orbital contribution is smaller for $[\mathbf{2_S}]^+$ than for $[\mathbf{1_S}]^+$. Our DFT studies also indicate that $quin^-$ exerts a stronger ligand-field effect than bpy.[13] Therefore, we now have shown that the conversion of the cobalt(II)–disulfide complex of L^2SSL^2 into cobalt(III)–thiolate compound $[\mathbf{2_S}]Cl$ can be achieved using an external ligand with large enough ligand-field strength, compensating for the lower ligand-field strength of L^2SSL^2.

Using DFT studies, we also revealed that the orientation of the asymmetric ligand $quin^-$ has a large effect on the stability of the thiolate compounds, as the experimentally obtained $[\mathbf{1_S}]^+$ is 6 kcal mol^{-1} more stable than hypothetical $[\mathbf{1_{S,rev}}]^+$ in methanol. This difference in stability is also observed for $[\mathbf{2_S}]^+$, which is 5 kcal mol^{-1} more stable than $[\mathbf{2_{S,rev}}]^+$. Activation strain and energy decomposition analyses show that the higher stability of $[\mathbf{1_S}]^+$ is caused by more favourable electrostatic interactions between the fragments $[Co(L^1S)]^{2+}$ and $[quin]^-$ in $[\mathbf{1_S}]^+$ compared to $[\mathbf{1_{S,rev}}]^+$. The positively charged $[Co(L^1S)]^{2+}$ fragment and the negatively charged $[quin]^-$ fragment are closer in $[\mathbf{1_S}]^+$ than in $[\mathbf{1_{S,rev}}]^+$, causing stronger electrostatic interactions in $[\mathbf{1_S}]^+$. These electrostatic interactions most likely are also present in the 'intermediate' compounds $[\mathbf{1_{SSquin}}]$ and $[\mathbf{2_{SSquin}}]$, resulting in the more favourable *mer* conformation of the ligand, making approach of the disulfide more facile and thus explaining the cleaner conversion of the disulfide compounds with $quin^-$ compared to bpy.

Conclusion

The cobalt(III)–thiolate complexes $[\mathbf{1_S}]Cl$ and $[\mathbf{2_S}]Cl$ can be formed from cobalt(II)–disulfide compound $[\mathbf{1_{SS}}]$ and $[\mathbf{2_{SS}}]$ in reactions with the anionic bidentate ligand 8-quinolinolate. Clean conversion of the disulfide compounds to their respective thiolate compounds was achieved in high yields due to the stronger ligand-field splitting energy caused by the ligand $quin^-$, as well as the seemingly preferential meridional orientation of L^1SSL^1 and L^2SSL^2 caused by the electrostatic interaction with the quinolinolate ligand. Our experimental results in combination with DFT calculations point out that by compensating the lower ligand-field strength of the ligand L^2SSL^2 with an exogenous strong-field ligand, conversion of the cobalt(II)–disulfide complex of L^2SSL^2 to the corresponding cobalt(III)–thiolate complex can indeed be achieved. It appears that the cobalt(III)–thiolate complex $[\mathbf{2_S}]Cl$ is involved in a concentration-dependent equilibrium with its redox dimer $[\mathbf{2_{SSquin}}]$. The Co(III)–thiolate complexes benefit from more stabilizing electrostatic interactions when the oxygen donor of $quin^-$ is located *trans* to the thiolate donor. Overall, this study suggests that the redox-conversion of Co(II)–disulfide compounds to Co(III)–thiolate complexes is affected largely by the ligand-field strength of both the disulfide ligand and the additional ligand. However, important parameters to consider may also comprise the charge of the added ligand and potentially stabilizing electrostatic interactions caused by the orientation of the auxiliary ligand. Further research will be directed to assess the magnitude of these effects using various ligand systems, and to further expand the investigations with different transition metal ions.

Experimental section

General

All reagents were purchased from commercial sources and were used as received unless noted otherwise. Degassed solvents used were obtained using the freeze–pump–thaw method followed by drying the solvents using the appropriate size of activated molecular sieves. The ligands L^1SSL^1, L^2SSL^2, and the cobalt compound $[Co_2(L^1SSL^1)Cl_4]$ $[\mathbf{1_{SS}}]$ were prepared according to previously published procedures.[2,10] The ligand L^2SSL^2 was purified similarly to the ligand L^1SSL^1, by refluxing in petroleum ether followed by cooling instead of using column chromatography as reported. The synthesis of the

cobalt compounds was performed using standard Schlenk-line techniques under an argon atmosphere. ^{1}H-NMR spectra were recorded on a Bruker 300 DPX spectrometer at room temperature. Mass spectra were recorded on a Thermo Scientific MSQ Plus and Shimadzu LCMS 2020 mass spectrometer with electrospray ionization (ESI) method. Formic acid was added to the eluting solvent with the final concentration of 1% (v/v). Simulated mass spectra were generated using mMass (version 5.5.0) software.[31] IR spectra were obtained using a PerkinElmer Spectrum Two System equipped with Universal ATR module containing diamond crystal for single reflection (scan range 400–4000 cm^{-1}, resolution 4 cm^{-1}). Magnetic susceptibility measurements were performed on a Sherwood Scientific Magnetic Susceptibility Balance MK1, and the magnetic moments were calculated according to the literature.[32] Bond distances and angles analysis of the crystal structures were performed using the Mogul module on Mercury (version 4.3.1) software.[33] UV-visible spectra were collected using a transmission dip probe with variable path lengths or a reflection probe on an Avantes AvaSpec-2048 spectrometer and using an Avalight-DH-S-Bal light source. Elemental analyses were performed by the Microanalytical Laboratory Kolbe in Germany.

Single crystal X-ray crystallography

All reflection intensities were measured at 110(2) K using a SuperNova diffractometer (equipped with Atlas detector) with either Mo Kα radiation (λ = 0.71073 Å) for [$\mathbf{2_{SSquin}}$] and [$\mathbf{2_S}$-Ag-$\mathbf{2_S}$]$(SbF_6)_3$ or Cu Kα radiation (λ = 1.54178 Å) for [$\mathbf{1_S}$]Cl under the program CrysAlisPro (Version CrysAlisPro 1.171.39.29c, Rigaku OD, 2017). The same program was used to refine the cell dimensions and for data reduction. The structure was solved with the program SHELXS-2018/3 (Sheldrick, 2018)[34] and was refined on F^2 with SHELXL-2018/3 (Sheldrick, 2018).[34] Numerical absorption correction based on Gaussian integration over a multifaceted crystal model for [$\mathbf{2_{SSquin}}$] and [$\mathbf{2_S}$-Ag-$\mathbf{2_S}$]$(SbF_6)_3$ was applied using CrysAlisPro. Analytical numeric absorption correction using a multifaceted crystal model for [$\mathbf{1_S}$]Cl was applied using CrysAlisPro. The temperature of the data collection was controlled using the system Cryojet (manufactured by Oxford Instruments). The H atoms were placed at calculated positions using the instructions AFIX 23, AFIX 43, AFIX 137, or AFIX147 with isotropic displacement parameters having values 1.2 or 1.5U_{eq} of the attached C or O atoms. The structure of compound [$\mathbf{1_S}$]Cl is ordered. The structure of [$\mathbf{2_{SSquin}}$] is partly disordered. The asymmetric unit also contains one partially occupied ordered lattice MeCN solvent molecule (occupancy factor: 0.903(7)) and some amount of significantly disordered lattice molecules (MeCN). The structure of [$\mathbf{2_S}$-Ag-$\mathbf{2_S}$]$(SbF_6)_3$ is significantly disordered (the Cobalt complex and three SbF_6^- counterions are mostly disordered). The asymmetric unit also contains one ordered lattice acetonitrile solvent molecule, and some amount of very disordered (and possibly partially occupied) lattice solvent molecules. The contributions of the very disordered solvent molecules in [$\mathbf{2_{SSquin}}$] and [$\mathbf{2_S}$-Ag-$\mathbf{2_S}$]$(SbF_6)_3$ were removed from the final refinement using the SQUEEZE procedure in Platon.[35,36] The crystal of [$\mathbf{2_S}$-Ag-$\mathbf{2_S}$]$(SbF_6)_3$ that was mounted on the diffractometer was twinned with two components, and the twin relationship corresponds to a twofold axis along the 0.0036$\mathbf{a^*}$ − 0.0009$\mathbf{b^*}$ + 1.0000$\mathbf{c^*}$ reciprocal direction. The BASF scale factor refines to 0.0483(6).

Computational methods

All calculations were performed with the Amsterdam Density Functional (ADF) program version 2017.103 using Zeroth Order Regular Approximation (ZORA) scalar relativistic effect at OPBE functional and TZP basis set for geometry optimizations and energies.[37–40] Solvation of the molecule was simulated using the conductor-like screening model (COSMO) in methanol.[41] The stationary points were checked to be minima at potential energy surface using vibrational analysis. All the compounds were calculated with S = 0, in agreement with our previous study.[13] Time-Dependent Density Functional Theory (TDDFT) calculations for the simulation of the UV-visible spectra were done using Davidson's procedure with ZORA scalar relativistic effect and conductor-like screening model (COSMO) in acetonitrile.[42] The calculations were done for the lowest 10 excitations of the Co(III)–thiolate compounds and lowest 30 excitations of the Co(II)–disulfide compounds. The simulated spectra have been adjusted for clearer comparison with the experimental data, the spectra were red-shifted for [$\mathbf{1_{SS}}$] (22 nm) and [$\mathbf{2_{SS}}$] (20 nm) and blue-shifted for $[\mathbf{1_S}]^+$ (66 nm) and $[\mathbf{2_S}]^+$ (60 nm). Kohn–Sham molecular orbital (KS-MO) analysis for the determination of d-orbital splitting energies of the complex was done according to the published procedure on the optimized geometries of $[\mathbf{1_S}]^+$ and $[\mathbf{2_S}]^+$ in the gas phase.[13]

Synthesis of the compounds

[$Co_2(L^2SSL^2)(Cl)_4$] ([$\mathbf{2_{SS}}$]). The compound was prepared similarly to compound [$\mathbf{1_{SS}}$],[10] using ligand L^2SSL^2 instead of L^1SSL^1. An intense purple powder was obtained in 72% yield. IR (neat, cm^{-1}): 3066w, 2924w, 1668w, 1605s, 1574 m, 1442s, 1381 m, 1364 m, 1298w, 1225w, 1159 m, 1090 m, 1053 m, 1017s, 960 m, 860 m, 765vs, 730 m, 646 m, 562w, 536w, 521w, 500w, 417 m. UV–Visible spectra in acetonitrile: 545 nm (ε = 1.5 × 10^3 M^{-1} cm^{-1}), 652 nm (ε = 8.5 × 10^2 M^{-1} cm^{-1}), 850–950 nm (ε < 100 M^{-1} cm^{-1}). ESI-MS found (calcd.) for [$\mathbf{2_{SS}}$ − $4Cl^-$ + $2HCOO^-$]$^{2+}$ m/z 376.2 (376.04) and for [$\mathbf{2_{SS}}$ − $2Cl^-$ + $HCOO^-$]$^+$ m/z 777.1 (777.05). Elemental analysis (%) for compound [$\mathbf{2_{SS}}$] ($C_{30}H_{36}Cl_4Co_2N_6S_2$), calcd C, 44.79; H, 4.51; N, 10.45; found C, 44.72; H, 4.49; N, 10.43.

[Co(L^1S)(8-quinolinolate)]Cl ([$\mathbf{1_S}$]Cl). The ligand L^1SSL^1 (52.35 mg, 0.101 mmol) was dissolved in 4 mL dry and deoxygenated methanol. Into the solution of the ligand, anhydrous $CoCl_2$ (26.25 mg, 0.202 mmol, 2 equiv. to the L^1SSL^1) was added. The resulting purple solution was stirred for 1 hour. In a separate flask under argon, 8-quinolinol (45.12 mg, 0.311 mmol) was added along with 44 μL of triethylamine (0.316 mmol, 1 equiv. to 8-quinolinol). Dry and deoxygenated methanol (1 mL) was added to dissolve the 8-quinolinol and triethylamine. From this solution, 680 μL (=0.202 mmol of

8-quinolinol, 2 equiv. to L^1SSL^1) was transferred to the purple solution of $[Co_2(L^1SSL^1)Cl_4]$. The color of the solution quickly changed into brown and the solution was stirred for 2 hours. The solution was further concentrated until approximately 1 mL was left in the flask. Into the flask, 10 mL dry and deoxygenated diethyl ether was added, resulting in the formation of a brown precipitate. The precipitate was then washed twice with 10 mL dry and deoxygenated diethyl ether, filtered, and then dried *in vacuo*. Yield: 96 mg, 0.193 mmol, 96%. Dark brown single crystals of compound [**1$_S$**]Cl were grown after 2 days using vapor diffusion of dry and deoxygenated diethyl ether into a solution of [**1$_S$**]Cl in a 1 : 1 mixture of dry and deoxygenated acetonitrile and methanol. IR (neat, cm^{-1}): 2945w, 2602 m, 2496 m, 1608w, 1570 m, 1497s, 1461s, 1444 m, 1397 m, 1376s, 1321s, 1284 m, 1223w, 1172 m, 1111 m, 1036 m, 905w, 851w, 819 m, 775 m, 748s, 719w, 626 m, 516s, 462 m, 448 m, 424 m. ESI-MS calcd for $[\mathbf{1_S}]^+$ *m*/*z* 461.08, found *m*/*z* 461.1. ^{1}H-NMR (300 MHz, CD_3CN, RT) δ (ppm): 1.29–1.33 (t, triethylamine·HCl), 1.84–1.87 (t, 2 H, N–CH_2–C**H$_2$**–S), 3.01–3.08 (q, triethylamine·HCl), 3.34–3.38 (t, 2H, N–C**H$_2$**–CH_2–S), 4.57–4.62 and 5.45–5.50 (d, 4H, py–C**H$_2$**–N), 6.87–6.90 (dd, 1H, *ortho*-C**H**-O(quin$^-$)), 7.06–7.09 (dd, 1H, *para*-C**H**-O(quin$^-$)), 7.13–7.17 (t, 2H, 2**H$_4$**(py)), 7.25–7.27 (dd, 2H, 2**H$_3$**(py)), 7.37–7.42 (t, 1H, *meta*-C**H**-O(quin$^-$)), 7.46–7.48 (d, 2H, 2**H$_6$**(py)), 7.85–7.88 (3H, m, *meta*-C**H**-N(quin$^-$) and 2**H$_5$**(py)), 8.50–8.53 (dd, 1H, *para*-C**H**-N(quin$^-$)), 9.04–9.06 (dd, 1H, *ortho*-C**H**-N(quin$^-$)). Elemental analysis (%) for compound [**1$_S$**]Cl·1.5 H_2O ($C_{23}H_{22}ClCoN_4OS$·1.5 H_2O), calcd C, 52.73; H, 4.81; N, 10.69; found C, 52.86; H, 4.67; N, 10.58.

[Co(L^{2}S)(8-quinolinolate)]Cl ([2$_S$]Cl). Compound [**2$_S$**]Cl was obtained using a similar procedure as for compound [**1$_S$**]Cl but using L^2SSL^2 instead of L^1SSL^1. Yield: 102 mg, 0.2 mmol, 99%. Dark brown single crystals of compound [**2$_S$-Ag-2$_S$**]$(SbF_6)_3$ were grown after two days using vapor diffusion of diethyl ether into an acetonitrile solution containing [**2$_S$**]Cl and 1 equivalent of $AgSbF_6$. IR (neat, cm^{-1}): 3391br, 2978w, 2603w, 2497w, 1608w, 1568 m, 1497s, 1462s, 1447 m, 1381s, 1322s, 1289w, 1225w, 1173w, 1111 m, 1067w, 1037 m, 960w, 902w, 830 m, 807 m, 776 m, 748s, 726w, 650 m, 624 m, 517s, 462w, 436w, 413w. ESI-MS calcd for $[\mathbf{2_S}]^+$ *m*/*z* 475.1, found *m*/*z* 475.3. ^{1}H-NMR (300 MHz, CD_3CN, RT): 1.26–1.31 (t, triethylamine·HCl), 1.78 (s, 3H, py-C**H$_3$**), 2.98–3.05 (q, triethylamine·HCl), 3.18–3.50 (m, 2H, (N–C**H$_2$**–CH_2–S and N–CH_2–C**H$_2$**–S, the other two protons overlaps with the solvent peaks at around 1.9 ppm)), 4.50–4.62, 5.43–5.48, and 5.75–5.80 (d, d, t, 4H, N–C**H$_2$**–py and N–C**H$_2$**–pyMe), 6.89–6.92 (d, 1H, *ortho*-C**H**-O(quin$^-$)), 6.92–6.95 (dd, 1H, **H$_5$**(pyMe)), 7.01–7.07 (td, 2H, 2**H$_3$**(py and pyMe)), 7.08–7.12 (t, 1H, *para*-C**H**-N(quin$^-$)), 7.27–7.29 (d, 1H, *para*-C**H**-O(quin$^-$)), 7.36–7.41 (t, 2H, *meta*-C**H**-N(quin$^-$) and *meta*-C**H**-O(quin$^-$)), 7.66–7.72 (t, 1H, **H$_5$**(py)), 7.75–7.82 (m, 2H, 2**H$_4$**(py and pyMe)), 8.47–8.50 (dd, 1H, **H$_6$**(py)), 9.26–9.29 (dd, 1H, *ortho*-C**H**-N(quin$^-$)). Elemental analysis (%) for [**2$_S$**]Cl·H_2O ($C_{24}H_{25}ClCoN_4OS$·H_2O), calcd C, 54.50; H, 4.95; N, 10.59; found C, 54.26; H, 4.79; N, 10.49.

[Co$_2$(L^{2}SSL^2)(8-quinolinolate)$_2$Cl$_2$] ([2$_{SSquin}$]). Dark brown single crystals of [**2$_{SSquin}$**] were grown within 5 hours using vapor diffusion of dry and deoxygenated diethyl ether into a solution of [**2$_S$**]Cl (50 mg mL^{-1}) in dry and deoxygenated acetonitrile or CD_3CN. IR (neat, cm^{-1}): 3411br, 3050w, 2973w, 2924w, 1601 m, 1566s, 1495s, 1463s, 1452s, 1382s, 1366s, 1325s, 1284 m, 1222 m, 1169w, 1156w, 1134w, 1108s, 1085 m, 1052 m, 1035w, 1016 m, 984w, 931w, 892w, 860w, 822 m, 801 m, 784 m, 760 m, 741s, 729s, 645 m, 604w, 560w, 526 m, 499 m, 470w, 417 m. UV-Vis (solid-state reflectance): 400 nm, 530 nm, and onset of a third absorbance starting at 800–1000 nm. ^{1}H-NMR spectrum of [**2$_{SSquin}$**] (300 MHz, CD_3OD, RT) was recorded from the range of −100 ppm to 100 ppm as well as from 0 ppm to 12 ppm, the latter shows peaks that are similar to those found in the ^{1}H-NMR spectrum of [**2$_S$**]Cl.

Conflicts of interest

There are no conflicts to declare.

Acknowledgements

We are grateful to Dr. Sipeng Zheng for the ESI-MS measurements.

References

1 D. L. Nosco, R. C. Elder and E. Deutsch, *Inorg. Chem.*, 1980, **19**, 2545–2551.
2 S. Itoh, M. Nagagawa and S. Fukuzumi, *J. Am. Chem. Soc.*, 2001, **123**, 4087–4088.
3 Y. Ueno, Y. Tachi and S. Itoh, *J. Am. Chem. Soc.*, 2002, **124**, 12428–12429.
4 L. K. Watanabe, Z. S. Ahmed, J. J. Hayward, E. Heyer, C. L. B. Macdonald and J. M. Rawson, *Organometallics*, 2022, **41**, 226–234.
5 E. C. Constable, C. E. Housecroft, M. Neuburger, J. R. Price and S. Schaffner, *Dalton Trans.*, 2008, 3795–3797.
6 H. Jeong, Y. Kang, J. Kim, B.-K. Kim and S. Hong, *RSC Adv.*, 2019, **9**, 9049–9052.
7 M. Gennari, D. Brazzolotto, S. Yu, J. Pecaut, C. Philouze, M. Rouzieres, R. Clerac, M. Orio and C. Duboc, *Chem. – Eur. J.*, 2015, **21**, 18770–18778.
8 M. Gennari, B. Gerey, N. Hall, J. Pecaut, M.-N. Collomb, M. Rouzieres, R. Clerac, M. Orio and C. Duboc, *Angew. Chem., Int. Ed.*, 2014, **53**, 5318–5321.
9 L. Wang, F. G. C. Reinhard, C. Philouze, S. Demeshko, S. P. de Visser, F. Meyer, M. Gennari and C. Duboc, *Chem. – Eur. J.*, 2018, **24**, 11973–11982.
10 F. Jiang, M. A. Siegler, X. Sun, L. Jiang, C. Fonseca Guerra and E. Bouwman, *Inorg. Chem.*, 2018, **57**, 8796–8805.
11 E. C. M. Ording-Wenker, M. van der Plas, M. A. Siegler, S. Bonnet, F. M. Bickelhaupt, C. Fonseca Guerra and E. Bouwman, *Inorg. Chem.*, 2014, **53**, 8494–8504.
12 F. Jiang, C. Marvelous, A. C. Verschuur, M. A. Siegler, S. J. Teat and E. Bouwman, *Inorg. Chim. Acta*, 2022, 120880.

13 C. Marvelous, L. de Azevedo Santos, M. A. Siegler, C. Fonseca Guerra and E. Bouwman, *Dalton Trans.*, 2022, **51**, 8046–8055.
14 F. Jiang, M. A. Siegler and E. Bouwman, *Inorg. Chem. Commun.*, 2018, **94**, 53–56.
15 S. L.-F. Chan, T. L. Lam, C. Yang, J. Lai, B. Cao, Z. Zhou and Q. Zhu, *Polyhedron*, 2017, **125**, 156–163.
16 S. S. Massoud, K. T. Broussard, F. A. Mautner, R. Vicente, M. K. Saha and I. Bernal, *Inorg. Chim. Acta*, 2008, **361**, 123–131.
17 K. J. Franz, L. H. Doerrer, B. Spingler and S. J. Lippard, *Inorg. Chem.*, 2001, **40**, 3774–3780.
18 S. Dey, T. K. Todorova, M. Fontecave and V. Mougel, *Angew. Chem., Int. Ed.*, 2020, **59**, 15726–15733.
19 D. G. Lonnon, D. C. Craig and S. B. Colbran, *Inorg. Chem. Commun.*, 2003, **6**, 1351–1353.
20 C.-Y. Zhu, Y.-Q. Zhang, R.-Z. Liao, W. Xia, J.-C. Hu, J. Wu, H. Liu and F. Wang, *Dalton Trans.*, 2018, **47**, 13142–13150.
21 C. Janiak, *J. Chem. Soc., Dalton Trans.*, 2000, 3885–3896.
22 T. Konno, T. Kawamoto, R. Kuwabara, T. Yoshimura and M. Hirotsu, *Chem. Lett.*, 2002, 304–305.
23 M. Tamura, N. Yoshinari, A. Igashira-Kamiyama and T. Konno, *Acta Crystallogr., Sect. E: Struct. Rep. Online*, 2007, **63**, M1641–U1629.
24 N. Yoshinari, Y. Chikamoto, M. Iwata, T. Kawamoto and T. Konno, *Bull. Chem. Soc. Jpn.*, 2006, **79**, 1066–1068.
25 N. Yoshinari, A. Igashira-Kamiyama and T. Konno, *Acta Crystallogr., Sect. E: Struct. Rep. Online*, 2006, **62**, M1229–M1231.
26 A. K. Pal, C. Li, G. S. Hanan and E. Zysman-Colman, *Angew. Chem., Int. Ed.*, 2018, **57**, 8027–8031.
27 F. M. Bickelhaupt and K. N. Houk, *Angew. Chem., Int. Ed.*, 2017, **56**, 10070–10086.
28 P. Vermeeren, S. C. C. Van Der Lubbe, C. Fonseca Guerra, F. M. Bickelhaupt and T. A. Hamlin, *Nat. Protoc.*, 2020, **15**, 649–667.
29 F. M. Bickelhaupt and E. J. Baerends, in *Reviews in Computational Chemistry*, 2000, vol. 15, pp. 1–86.
30 J. T. Yarranton and J. K. McCusker, *J. Am. Chem. Soc.*, 2022, **144**, 12488–12500.
31 M. Strohalm, *mMass – Open Source Mass Spectrometry Tool*, **https://www.mmass.org**.
32 G. A. Bain and J. F. Berry, *J. Chem. Educ.*, 2008, **85**, 532–536.
33 C. F. Macrae, I. Sovago, S. J. Cottrell, P. T. A. Galek, P. McCabe, E. Pidcock, M. Platings, G. P. Shields, J. S. Stevens, M. Towler and P. A. Wood, *J. Appl. Crystallogr.*, 2020, **53**, 226–235.
34 G. M. Sheldrick, *Acta Crystallogr., Sect. A: Found. Crystallogr.*, 2008, **64**, 112–122.
35 A. L. Spek, *Acta Crystallogr., Sect. C: Struct. Chem.*, 2015, **71**, 9–18.
36 A. L. Spek, *Acta Crystallogr., Sect. D: Biol. Crystallogr.*, 2009, **65**, 148–155.
37 M. Swart, A. W. Ehlers and K. Lammertsma, *Mol. Phys.*, 2004, **102**, 2467–2474.
38 *ADF2017.107, SCM Theoretical Chemistry*, Vrije Universiteit, Amsterdam, The Netherlands, **https://www.scm.com**.
39 E. Van Lenthe and E. J. Baerends, *J. Comput. Chem.*, 2003, **24**, 1142–1156.
40 E. Van Lenthe, E. J. Baerends and J. G. Snijders, *J. Chem. Phys.*, 1994, **101**, 9783–9792.
41 A. Klamt and G. Schuurmann, *J. Chem. Soc., Perkin Trans. 2*, 1993, 799–805.
42 A. Rosa, E. J. Baerends, S. J. A. van Gisbergen, E. van Lenthe, J. A. Groeneveld and J. G. Snijders, *J. Am. Chem. Soc.*, 1999, **121**, 10356–10365.